Excitation of Propagating Plasmons in a Periodic Graphene Structure by Incident Terahertz Waves

D.V. Fateev,[1,2,*] K.V. Mashinsky,[1] O.V. Polischuk,[1] and V.V. Popov[1]

[1]*Kotelnikov Institute of Radio Engineering and Electronics, Russian Academy of Sciences, Saratov 410019, Russia*
[2]*Saratov State University, Saratov 410012, Russia*

The transformation of an electromagnetic wave into a propagating plasmon in a periodical dual-grating-gated graphene structure is theoretically investigated. The electromagnetic wave is incident at normal direction upon the structure. The most effective transformation appears in two cases: (i) a combined excitation of the radiative and "nonradiative" gated plasmon modes and (ii) excitation of the plasmon modes with the wavevectors in multiples of the structure inverse period. We find a 70% transformation of the incident power into a propagating plasmon for a 1-ps carrier momentum relaxation time in graphene when canceling the transmission of the electromagnetic wave through the graphene structure by a metallic ground plate and blocking the reflection with a Fabry-Perot resonator.

I. INTRODUCTION

Graphene is a perspective media for excitation and investigation of the plasmons in the terahertz (THz) frequency range [1–5]. Graphene may be used in the van der Waals structures [6]. Encapsulating graphene between two films of hexagonal boron nitride (*h*-BN) provides a high-quality plasmon medium [7] with high charge-carrier mobility around $100\,000$ cm^2/(V s) at room temperature [8,9]. The momentum relaxation time of charge carriers in graphene reaches the value of 2 ps at room temperature [10,11].

It has been suggested that the plasmon properties of a periodical graphene structure are used to amplify [12], detect [13], and transform THz waves [14]. Coupling of plasma waves in graphene [15,16] to incident electromagnetic waves demands special couplers that balance different momenta of the incident electromagnetic wave and the plasmon. Typically, wide-area couplers to be used for exciting standing THz plasmon in graphene are periodical one-dimensional [17–19] and two-dimensional [20,21] gratings. Unlike periodic systems, in which the diffraction of electromagnetic waves is investigated [22], slow plasmon modes are excited in short-period structures in which higher diffraction harmonics are nondiffractive (evanescent). Plasmon excitation in such wide-area graphene structures can be identified via absorption of the energy of incident electromagnetic waves. The perfect absorption of incident waves was found in a periodic graphene structure with a metallic ground plate due to utilizing the Fabry-Perot conditions for reflected waves [23].

In order to excite the propagating plasmon, different methods can be used: diffraction of incident waves on the cantilever of a scanning near-field microscope [24–28], on a single metal gate [29], or on a slit in a metal gate [30] that is placed over graphene. The traveling plasmon mode can be excited in a graphene structure with a periodic metal grating gate and dc drift current in graphene [31] or by using a magneto-optical substrate [32]. The effect of attenuated total reflection is proposed for an excitation traveling plasmon in graphene [33,34]. Also, the compression of surface polaritons in tapered bulk slabs is proposed to transform an electromagnetic wave into a propagating plasmon [35]. The excitation of the unidirectionally propagating plasmon can be possible due to the interference of two plasmons excited by two nanoridges in graphene [36]. All optical generation of graphene plasmons can be accomplished without local scatters by manipulating the phase matching conditions [37]. The drawbacks of the methods mentioned above are low transformation efficiency for diffraction methods and strong dependence on the incident angle for attenuated total reflection methods.

In this work, we propose the periodic graphene structure with a dual-grating gate (DGG) and asymmetric unit cell as an effective transformer of normally incident THz electromagnetic wave into a propagating plasmon in graphene. The asymmetric DGG ensures the conservation of momentum for excitation of propagating plasmon by the incident THz wave. We theoretically demonstrate that transformation of an incident wave into a propagating plasmon exceeds 70% for realistic parameters of the structure for

_____
*fateevdv@yandex.ru

room temperature in the DGG graphene structure with a metallic back gate in the case of blocking the reflectance by a Fabry-Perot resonator.

II. THEORETICAL MODEL

The DGG structure under consideration is shown in Fig. 1. The homogeneous graphene layer is separated from the DGG by a thin dielectric slab with thickness d. The graphene layer is screened by a spatially homogeneous metallic back gate. The thickness of a dielectric slab between the graphene and the back gate is h. The THz electromagnetic wave with the electric field polarized across the DGG fingers is normally incident from the top onto the metal DGG. The DGG consists of two periodical interdigitated subgratings. Two subgratings of the DGG are laterally shifted with respect to each other in order to introduce an asymmetry into the unit cell of the periodic DGG graphene structure. In structures with two-dimensional (2D) plasmons excited via diffraction of electromagnetic waves on the DGG with an asymmetric unit cell, a noncentrosymmetric electric field can be induced [38]. The in-plane noncentrosymmetric electric fields in the DGG structure with a 2D electron gas trigger the plasmonic effect of electron drag in the 2D electron gas [13,38,39], which was studied in the experiment in Ref. [40].

We solve the problem of the excitation of plasmon modes in a DGG graphene structure within a self-consistent electromagnetic approach using the full system of the Maxwell equations. The solving of the electromagnetic problem consists of transforming the Maxwell equations and boundary conditions into the spatial Fourier representation, then formulating the integral equations with respect to the surface currents in DGG strips, and numerically solving the integral equations by the Galerkin procedure with the expansion of surface currents into series

on the Legendre polynomials (for a description of the electromagnetic approach, see the Appendix; for details of a similar approach, also see Ref. [41]). The THz response of graphene is described by the dynamic conductivity [42,43] described by Eq. (A4) in the Appendix with a Fermi energy of 150 meV. All results shown here are calculated for the sum of the DGG openings $s_1 + s_2 = 350$ nm, width $w_2 = 500$ nm, and the sum of the dielectric slabs thicknesses $d + h = 6$ μm.

The electromagnetic energy flux in the graphene structure is described by the time-averaged Poynting vector $\mathbf{S} = \frac{1}{2}\text{Re}[\mathbf{EH}^*]$, where $\mathbf{E}$ is the total electric field and $\mathbf{H}$ is the total magnetic field. We investigate the excitation of the plasmons in a DGG graphene structure [Fig. 1(b)] by the TM electromagnetic wave of the DGG and, therefore, the energy flux has only two components: $S_x = -\frac{1}{2}\text{Re}\left(E_z H_y^*\right)$ and $S_z = \frac{1}{2}\text{Re}\left(E_x H_y^*\right)$.

The incident flux of a normally incident THz wave is

$$S_z^{\text{inc}} = -\frac{1}{2}\sqrt{\frac{\varepsilon_1 \varepsilon_0}{\mu_0}}\left|E_x^{\text{inc}}\right|^2, \tag{1}$$

where E_x^{inc} is the electric field of the incident wave, ε_1 is the dielectric constant of the upper medium (air), and ε_0 and μ_0 are the electric and magnetic constants respectively.

For a spatially periodic structure, the electric and magnetic fields can be expanded into Fourier series as $E_x(x, z, t) = \sum_{p=-\infty}^{\infty} e_{x,p}(z)\exp\left(iq_p x - i\omega t\right)$, where $e_{x,p}(z)$ is the Fourier amplitude of the x component of the electric field, $q_p = 2\pi p/L$ is the reciprocal vector with p being an integer, and ω is the frequency of the incident THz wave.

The energy flux in the x direction caused by a propagating plasmon is given by averaging over the spatial period of the structure and integrating over the z coordinate the x
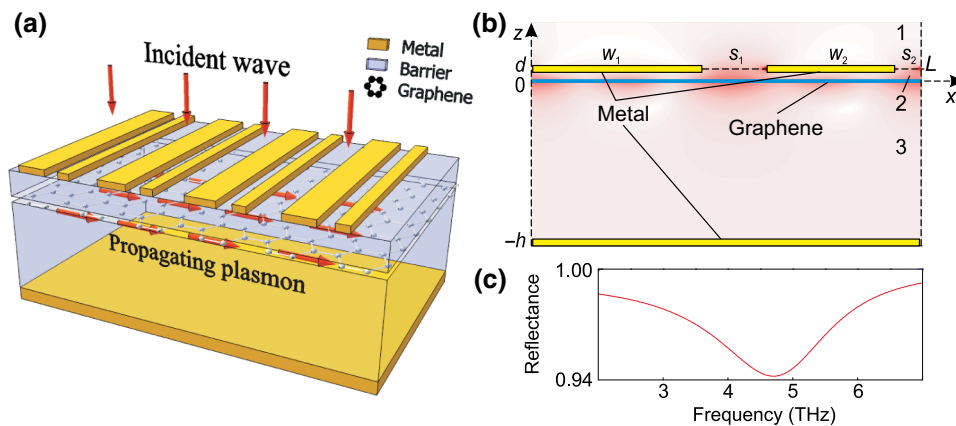

FIG. 1. (a) Schematic view of the DGG graphene structure. (b) One unit cell of the DGG graphene structure. A typical spatial distribution of a plasmon electric field in the unit cell of the DGG graphene structure is shown. (c) Fabry-Perot resonance for the graphene structure without DGG.

component of the Poynting vector

$$S_x^P = \frac{1}{L} \int_{-h}^{+\infty} \int_0^L S_x \, dx \, dz, \qquad (2)$$

where L is the spatial period of the structure. This plasmon energy flux is composed of three terms, $S_x^P = S_x^{P1} + S_x^{P2} + S_x^{P3}$, where

$$S_x^{P1} = \frac{\omega \varepsilon_1 \varepsilon_0}{4} \sum_{p \neq 0} \frac{q_p}{\left| q_{z,p}^{(1)} \right|^2} \frac{\beta_p^{(1)} \left| e_{x,p}^{(1)} \right|^2}{\mathrm{Im}\left(q_{z,p}^{(1)} \right)},$$

$$S_x^{P2} = \frac{\omega \varepsilon_2 \varepsilon_0}{4} \sum_{p \neq 0} \frac{q_p}{\left| q_{z,p}^{(2)} \right|^2} \frac{\beta_p^{(2,2)} \left| e_{x,p}^{(2,2)} \right|^2 - \beta_p^{(2,1)} \left| e_{x,p}^{(2,1)} \right|^2}{\mathrm{Im}\left(q_{z,p}^{(2)} \right)}$$

$$- \omega \varepsilon_2 \varepsilon_0 d \sum_{p \neq 0} \frac{q_p}{\left| q_{z,p}^{(2)} \right|^2} \mathrm{Re}\left[e_{x,p}^{(2,1)} \left(e_{x,p}^{(2,2)} \right)^* \right],$$

$$S_x^{P3} = \frac{\omega \varepsilon_3 \varepsilon_0}{4} \sum_{p \neq 0} \frac{q_p}{\left| q_{z,p}^{(3)} \right|^2} \frac{\beta_p^{(3,2)} \left| e_{x,p}^{(3,2)} \right|^2 - \beta_p^{(3,1)} \left| e_{x,p}^{(3,1)} \right|^2}{\mathrm{Im}\left(q_{zp}^{(3)} \right)}$$

$$- \omega \varepsilon_3 \varepsilon_0 h \sum_{p \neq 0} \frac{q_p}{\left| q_{z,p}^{(3)} \right|^2} \mathrm{Re}\left[e_{x,p}^{(3,1)} \left(e_{x,p}^{(3,2)} \right)^* \right],$$

where

$$\beta_p^{(1)} = \exp\left[-2\mathrm{Im}\left(q_{z,p}^{(1)} \right) d \right],$$

$$\beta_p^{(2,n)} = \exp\left[(-1)^n 2\mathrm{Im}\left(q_{z,p}^{(2)} \right) d \right] - 1,$$

$$\beta_p^{(3,n)} = 1 - \exp\left[(-1)^{n+1} 2\mathrm{Im}\left(q_{z,p}^{(3)} \right) h \right].$$

We use the dependencies of the induced electric fields in different media on the z coordinate [see Fig. 1(b)] as Eq. (A1) from the Appendix. Here, $q_{z,p}^{(\alpha)} = \sqrt{\omega^2 \varepsilon_\alpha \varepsilon_0 \mu_0 - q_p^2}$ (for $\alpha = 1, 2, 3$) are the transversal wavevectors of the spatial Fourier harmonics in different dielectric media and ε_α are the dielectric constants of the dielectric media. In case of the plasmon excitation in graphene by a short-period DGG, all transversal wavevectors with $|p| > 0$ are imaginary and the transversal wavevector with $p = 0$ is real. Therefore, all Fourier harmonics with $|p| > 0$ are the evanescent waves and the reflected THz wave is described by the spatial harmonic with $p = 0$. Then the Poynting flux of the reflected wave is

$$S_z^R = \frac{1}{2} \sqrt{\frac{\varepsilon_1 \varepsilon_0}{\mu_0}} \left| e_{x,0}^{(1)} \right|^2. \qquad (3)$$

Then the reflectance coefficient is

$$R = \frac{S_z^R}{\left| S_z^{\mathrm{inc}} \right|}, \qquad (4)$$

and the absorbance coefficient is $A = 1 - R$. We introduce the coefficient of transformation of the incident wave into the propagating plasmon as

$$T_P = \frac{S_x^P}{\left| S_{L,z}^{\mathrm{inc}} \right|}, \qquad (5)$$

where $S_{L,z}^{\mathrm{inc}} = L S_z^{\mathrm{inc}}$ is the Poynting flux incident onto one unit cell of the periodic DGG structure.

We calculate the velocity of the energy of the propagating plasmon as

$$v_s = \frac{S_x^P}{W_{LT}}, \qquad (6)$$

where W_{LT} is the spatiotemporal averaged energy density of the electric and magnetic fields of the plasmon. For the DGG graphene structure, the spatiotemporal averaged energy density of the electric and magnetic fields of the plasmon can be written as $W_{LT} = W_{LT}^{(1)} + W_{LT}^{(2)} + W_{LT}^{(3)}$, where

$$W_{LT}^{(1)} = \frac{\varepsilon_1 \varepsilon_0}{8} \sum_{p \neq 0} \xi_p^{(1)} \frac{\beta_p^{(1)} \left| e_{x,p}^{(1)} \right|^2}{\mathrm{Im}\left(q_{z,p}^{(1)} \right)},$$

$$W_{LT}^{(2)} = \frac{\varepsilon_2 \varepsilon_0}{8} \sum_{p \neq 0} \xi_p^{(2)} \frac{\beta_p^{(2,2)} \left| e_{x,p}^{(2,2)} \right|^2 - \beta_p^{(2,1)} \left| e_{x,p}^{(2,1)} \right|^2}{\mathrm{Im}\left(q_{z,p}^{(2)} \right)}$$

$$+ \frac{\varepsilon_2 \varepsilon_0 d}{2} \sum_{p \neq 0} \zeta_p^{(2)} \mathrm{Re}\left[e_{x,p}^{(2,1)} \left(e_{x,p}^{(2,2)} \right)^* \right],$$

$$W_{LT}^{(3)} = \frac{\varepsilon_3 \varepsilon_0}{8} \sum_{p \neq 0} \xi_p^{(3)} \frac{\beta_p^{(3,2)} \left| e_{x,p}^{(3,2)} \right|^2 - \beta_p^{(3,1)} \left| e_{x,p}^{(3,1)} \right|^2}{\mathrm{Im}\left(q_{z,p}^{(3)} \right)}$$

$$+ \frac{\varepsilon_3 \varepsilon_0 h}{2} \sum_{p \neq 0} \zeta_p^{(3)} \mathrm{Re}\left[e_{x,p}^{(3,1)} \left(e_{x,p}^{(3,2)} \right)^* \right],$$

with

$$\xi_p^{(\alpha)} = 1 + \frac{\omega^2 \varepsilon_\alpha \varepsilon_0 \mu_0 + q_p^2}{\left| q_{z,p}^{(\alpha)} \right|^2},$$

$$\zeta_p^{(\alpha)} = 1 - \frac{\omega^2 \varepsilon_\alpha \varepsilon_0 \mu_0 + q_p^2}{\left| q_{z,p}^{(\alpha)} \right|^2}.$$

In order to enhance the interaction of the incident THz wave with graphene, we cancel the transmission of the

THz wave through the DGG structure by using a homogeneous metallic back gate and weaken the reflection from the DGG structure by using the Fabry-Perot conditions for the reflected wave. By varying the thickness h, we can tune the frequency of the Fabry-Perot resonance to the frequencies of excited plasmon modes. The Fabry-Perot resonance for the graphene structure without the DGG is shown in Fig. 1(c). The presence of the DGG shifts the frequency of the Fabry-Perot resonance. Therefore, we examine the DGG graphene structure, looking for maximum values of absorbance near the frequency of the Fabry-Perot resonance for the graphene structure without DGG.

III. RESULTS AND DISCUSSION

In the DGG graphene structure, it is possible to excite the gated plasmon modes with wave numbers quantized as $k_x = \pi n / w_l$ (for $l = 1, 2$), where w_l are the widths of the fingers of different DGG subgratings and $n = 1, 2, 3, \ldots$. In the spatially symmetrical structure, only "bright" plasmon modes with odd numbers $n = 1, 3, 5, \ldots$ can be excited, while for the excitation of "dark" plasmon modes with even numbers $n = 2, 4, 6, \ldots$, spatial asymmetry of the unit cell of the periodic structure is needed.

The resonantly excited gated plasmon under gate w_1 and forced plasmon under gate w_2 have a weak asymmetry of the spatial distribution of the electric field. Hence, we consider the conditions of excitation of the "hybrid" plasmon mode, which consists of a simultaneously resonantly excited gated plasmon with $n = 1$ under gate w_1 and a gated plasmon with $n = 2$ under the gate w_2. Such hybrid plasmon modes have enhanced asymmetry of the plasmon electric fields in graphene [see the electric field distribution near the dashed line in Fig. 2(c)], which leads to the effective excitation of the traveling plasmon modes.

We examine the interaction of the gated plasmon modes close to the Fabry-Perot resonance, optimizing every geometrical parameter of the DGG graphene structure. Keeping the width of the gate w_2, the frequency of the Fabry-Perot resonance, and the sum of $s_1 + s_2$ unchanged and optimizing the asymmetry coefficient $K = 1 - s_1/s_2$, we calculate the absorbance A and transformation coefficient T_p [see Figs. 2(a) and 2(b)]. In the regime of interaction of the fundamental plasmon mode with index $n_1 = 1$ and dark plasmon mode with index $n_2 = 2$, the transformation of an incident wave into a propagating plasmon reaches the value of 51% [Fig. 2(b)] for the carrier momentum relaxation time in graphene $\tau = 1$ ps. The absorbance reaches the value of 0.9996 at the point of the maximum transformation coefficient T_p [Fig. 2(a)] due to the Fabry-Perot resonance of the electromagnetic wave. The transformation coefficient for this hybrid gated plasmon mode at the frequency of 4 THz reaches its maximum value for the asymmetry coefficient $K = 0.6$. The distribution of the in-graphene-plane component of the electric field at the maximum transformation point clearly demonstrates the interaction of the fundamental plasmon mode with index $n_1 = 1$ under the gate w_1 and dark plasmon mode with index $n_2 = 2$ under the gate w_2 [Fig. 2(c)]. The calculated velocity of the propagating plasmon is $v_s = 1.27 \times 10^6$ m/s; then the mean free pass (MFP) can be estimated as $l_{\mathrm{MFP}} = v_s \tau$, which equals 1.27 μm.

The physical mechanism of the excitation of a propagating plasmon in a periodic graphene structure is connected with the excitation of the dark plasmon modes with an odd (asymmetric) spatial distribution of the longitudinal component of the electric field with respect to the center of the plasmon cavity. The dark plasmon modes are described by the sum of the Fourier harmonics traveling in opposite directions, which have unequal amplitudes in pairs of the same order. In a situation where the amplitudes of
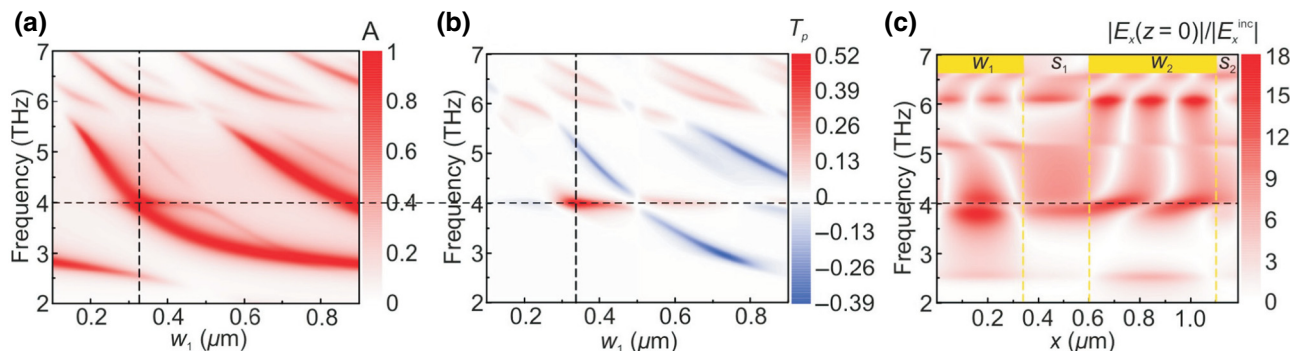

FIG. 2.   Transformation of an incident THz wave into a propagating plasmon mode for $w_2 = 500$ nm, $d = 25$ nm, $d + h = 6$ μm, and $K = 0.6$. (a) Spectra of absorbance A depending on the width of the gate finger w_1. (b) Spectra of the transformation coefficient T_p depending on the width of the gate finger w_1. The point of maximum transformation is shown by the cross of the dashed straight lines. (c) Spatial distribution of the x component of the electric field over the unit cell of the DGG graphene structure at the point of maximum transformation frequency for $w_1 = 0.34$ μm and frequency 4 THz.
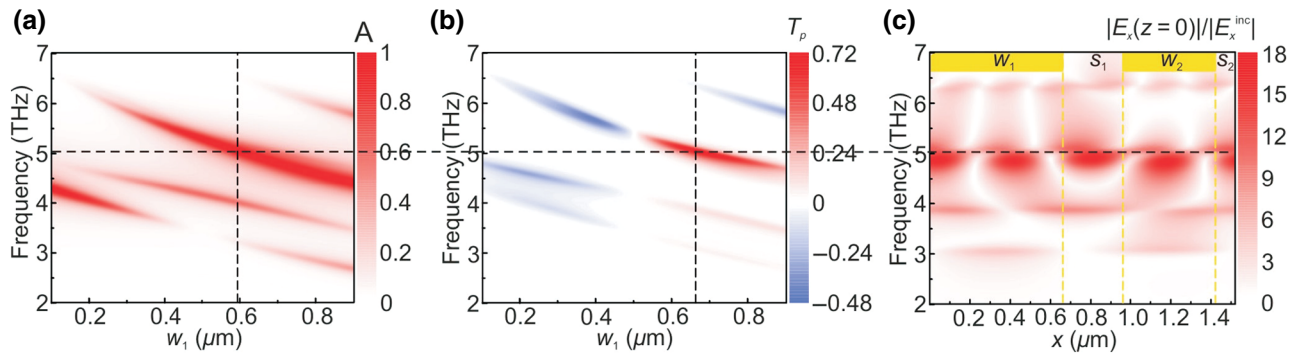
FIG. 3. Transformation of an incident THz wave into a propagating plasmon mode for $w_2 = 500$ nm, $d = 105$ nm, $d + h = 6$ μm, and $K = 0.7$. (a) Spectra of absorbance A depending on the width of the gate finger w_1. (b) Spectra of transformation coefficient T_p depending on the width of the gate finger w_1. The point of maximum transformation is shown by the cross of the dashed straight lines. (c) Spatial distribution of the x component of the electric field over the unit cell of the DGG graphene structure at the point of maximum transformation frequency for $w_1 = 0.672$ μm and frequency 5.025 THz.

the Fourier harmonics differ significantly, the propagating plasmon arises.

Fabry-Perot resonance also allows for increasing the transformation coefficient T_p for plasmon modes with wave numbers quantized as $k_x = 2\pi n/L$ (where n is an integer) [Fig. 3(a)]. Such plasmon modes can be excited when the distance between the DGG and graphene is comparable to (or greater than) DGG finger widths. Using the optimization process (similar to that for the gated plasmons), we find a maximum transformation coefficient of 71.5% [Fig. 3(b)] for a 1-ps carrier momentum relaxation time in the case of excitation of the plasmon mode with wave number $k_x = 4\pi/L$. The absorbance reaches the value of 0.9996 at the point of the maximum transformation coefficient T_p [Fig. 3(a)] due to the Fabry-Perot resonance of an electromagnetic wave. The transformation coefficient for this plasmon mode reaches its maximum value for the asymmetry coefficient of $K = 0.7$. The distribution of the in-graphene-plane component of the electric field at the maximum transformation point corresponds to the excitation of a spatially asymmetric plasmon mode with $k_x = 4\pi/L$ [Fig. 3(c)]. In such a case, the calculated velocity of the propagating plasmon is $v_s = 3.77 \times 10^6$ m/s, which gives the mean free pass 3.77 μm.

By varying the position of graphene in Fabry-Perot slab (varying d and keeping the sum $d + h$ constant) and optimizing other geometrical parameters, we establish two optimum distances d for the best transformation of the THz wave into the propagating plasmon (Fig. 4). Figure 4 is obtained following the evolution of the maximum transformation points in Figs. 2(b) and 3(b) by varying the position of graphene in the Fabry-Perot slab. The first maximum at small distance $d = 25$ nm corresponds to the most effective excitation of gated plasmon modes in the structure (Fig. 2). The second maximum at $d = 105$ nm corresponds to the most effective excitation of the plasmon modes with the wave number $k_x = 4\pi/L$ (Fig. 3). Further increasing d

is inexpedient since, for greater d, the evanescent fields of the DGG weakly excite plasmons in graphene (the decay length of the plasmon electric field in the z direction is determined by the plasmon wavelength $\lambda_p \propto L/n$, where n is the index of the plasmon mode [44]).

Now, we investigate the dependence of the transformation coefficient on the carrier momentum relaxation time for both types of plasmon modes (Fig. 5). The transformation coefficient T_p for a plasmon mode with wave number $k_x = 4\pi/L$ ($d = 105$ nm) reaches greater values in comparison with that for the gated plasmon modes ($d = 25$ nm). Each transformation coefficient reaches its maximum at the value of the relaxation time (Fig. 5), which corresponds to the optimum coupling between the DGG structure and the incident THz wave [45]. Estimations of the mean free paths for optimum values of the momentum relaxation times give 2.03 μm for the gated plasmon mode and 15.39 μm for the plasmon modes with wave number $k_x = 4\pi/L$ (Fig. 5). Because of such long mean
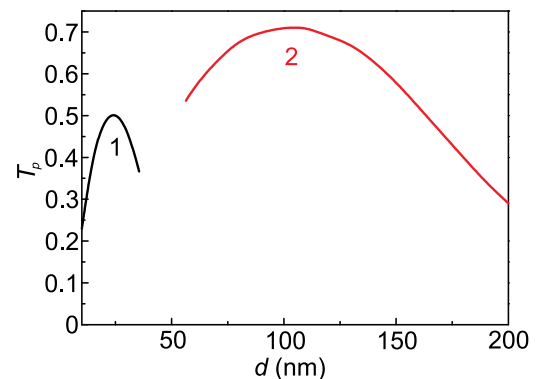

FIG. 4. Dependence of the transformation coefficient for the gated plasmon modes (black curve 1) and plasmon modes with $k_x = 4\pi/L$ (red curve 2) on distance d, keeping the sum $d + h$ constant as $d + h = 6$ μm.
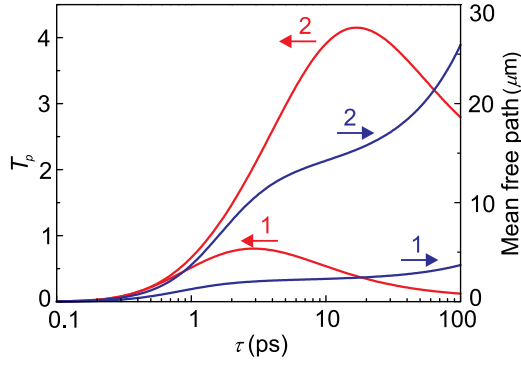
FIG. 5. Dependence of the transformation coefficient T_p (red) and mean free paths (blue) for the gated plasmon modes (1) and plasmon modes with $k_x = 4\pi/L$ (2) on the carrier momentum relaxation time τ. Curves 1 are calculated for $w_1 = 0.34$ μm, $d = 25$ nm, $K = 0.6$, and frequency 4 THz. Curves 2 are calculated for $w_1 = 0.672$ μm, $d = 105$ nm, $K = 0.7$, and frequency 5.025 THz.

free paths in comparison with period of the structure, the energy of the propagating plasmon is not fully absorbed at the unit cell of the periodic structure, but overflows into the neighboring unit cells. Because of that, the transformation coefficients can exceed unity.

IV. CONCLUSION

It is possible to transform a normally incident electromagnetic wave into a propagating plasmon in graphene using the DGG structure with an asymmetric unit cell. Screening the structure with the back metal gate and Fabry-Perot blocking of reflectance from the DGG structure allows for increasing the efficiency of the transformation of the incident wave into a propagating plasmon. The maximum of the transformation occurs for two types of the plasmon modes: the gated plasmon modes and plasmon modes with wave number in multiples of the structure inverse period. Periodical structures with an asymmetric unit cell can be utilized as transformers of the incident electromagnetic wave into propagating plasmons.

ACKNOWLEDGMENTS

APPENDIX: ELECTROMAGNETIC APPROACH

We represent the DGG graphene structure (Fig. 1 of the paper) by a model shown in Fig. 1(b). All elements of the structure are spatially homogeneous in the y direction. We investigate the DGG graphene structure with a spatially homogeneous graphene and back gate. The electromagnetic wave with components of electric E_x^{inc} and magnetic field H_y^{inc} is incident normally from the top onto the DGG

and excites the TM polarized diffracted electromagnetic field (with nonzero components of the electric field E_x, E_z, and magnetic field H_y). The DGG is represented by infinitely thin layers with surface conductivity equal to the surface conductivity of gold. The back gate is modeled by a perfect conductor.

The basic steps of electromagnetic approach are described below.

In the first step, we write the Maxwell equations in three media in a Fourier representation. It means that all components of the electric and magnetic fields are expanded into Fourier series as $H_y(x, z, t) = \sum_{p=-\infty}^{\infty} h_{y,p}(z) \exp(iq_p x - i\omega t)$, where H_y is the y component of the magnetic field and $h_{y,p}(z)$ are the Fourier amplitudes of the magnetic field. We use the dependencies of the induced electric fields in different media on the z coordinate [see Fig. 1(b)] as

$$e_{x,p}^{(1)}(z) = e_{x,p}^{(1)} \exp\left(iq_{z,p}^{(1)}z\right),$$

$$e_{x,p}^{(2)}(z) = e_{x,p}^{(2,1)} \exp\left(iq_{z,p}^{(2)}z\right) + e_{x,p}^{(2,2)} \exp\left(-iq_{z,p}^{(2)}z\right), \quad \text{(A1)}$$

$$e_{x,p}^{(3)}(z) = e_{x,p}^{(3,1)} \exp\left(iq_{z,p}^{(3)}z\right) + e_{x,p}^{(3,2)} \exp\left(-iq_{z,p}^{(3)}z\right),$$

where $e_{x,p}^{(\alpha)}(z)$ are the Fourier amplitudes of the electric field in different dielectric media. Then, we apply the boundary conditions in the planes $z = d$, $z = 0$, and $z = -h$, which in the Fourier representation can be written as

$$\begin{cases} e_{x,p}^{(1)}(d) + \delta_{p,0}E_x^{\text{inc}}(d) = e_{x,p}^{(2)}(d), \\ h_{y,p}^{(1)}(d) + \delta_{p,0}H_x^{\text{inc}}(d) - h_{y,p}^{(2)}(d) = -j_{x,p}(d), \end{cases}$$

$$\begin{cases} e_{x,p}^{(2)}(0) = e_{x,p}^{(3)}(0), \\ h_{y,p}^{(2)}(0) - h_{y,p}^{(3)}(0) = -j_{x,p}(0), \end{cases} \quad \text{(A2)}$$

$$\begin{cases} e_{x,p}^{(3)}(-h) = 0, \end{cases}$$

where $j_{x,p}(z)$ are the Fourier harmonics of the current densities in the planes $z = d$ and $z = 0$.

The Fourier harmonics of the electric fields and current densities in spatially homogeneous graphene are connected by the Fourier-transformed Ohm's law as

$$j_{x,p}(0) = \sigma_{\text{gr}}(\omega)e_{x,p}^{(2)}(0), \quad \text{(A3)}$$

where

$$\sigma_{\text{gr}}(\omega) = \frac{e^2 2\tau k_B T}{\pi \hbar^2 (1 - i\omega\tau)} \ln\left[2\cosh\left(\frac{\mathcal{E}_F}{2k_B T}\right)\right]$$
$$+ \frac{e^2}{4\hbar^2} Q\left(\frac{\hbar\omega}{2}\right)$$
$$- \frac{e^2\omega}{i\pi} \int_0^\infty \frac{Q(\mathcal{E}) - Q\left(\frac{\hbar\omega}{2}\right)}{\hbar^2\omega^2 - 4\mathcal{E}^2} d\mathcal{E} \quad \text{(A4)}$$

is the frequency-dependent conductivity of graphene [42, 43], with

$$Q(\vartheta) = \frac{\sinh\left(\frac{\vartheta}{k_B T}\right)}{\cosh\left(\frac{\vartheta}{k_B T}\right) + \cosh\left(\frac{\mathcal{E}_F}{k_B T}\right)}.$$

Here, $\mathcal{E}_F$ is the Fermi energy in graphene, T is the temperature, e is the electron charge, and k_B is the Boltzmann constant. Then using the Maxwell equations and boundary conditions (A2), we obtain the equations

$$e_{x,p}^{(1)}(d) = Z_p(\sigma_{\mathrm{gr}})j_d$$
$$- \left(2\sqrt{\frac{\varepsilon_0 \varepsilon_1}{\mu_0}} Z_0(\sigma_{\mathrm{gr}}) e^{-id\omega\sqrt{\varepsilon_0\mu_0\varepsilon_1}} + 1\right)\delta_{p,0}E_x^{\mathrm{inc}},$$
(A5)

where

$$Z_p(\sigma_{\mathrm{gr}}) = \frac{q_{z,p}^{(1)} q_{z,p}^{(2)}\left(\eta_1\eta_5 q_{z,p}^{(2)} - \eta_2\eta_6 q_{z,p}^{(3)}\right)}{\varepsilon_0\omega\chi}$$

are the Fourier impedances of the graphene structure in the DGG plane, with

$$\chi = \eta_6 q_{z,p}^{(3)}\left(\eta_2 q_{z,p}^{(2)}\varepsilon_1 - \eta_1 q_{z,p}^{(1)}\varepsilon_2\right)$$
$$- \eta_5 q_{z,p}^{(2)}\left(\eta_1 q_{z,p}^{(2)}\varepsilon_1 - \eta_2\varepsilon_2 q_{z,p}^{(1)}\right),$$
$$\eta_1 = -1 + \exp\left(2idq_{z,p}^{(2)}\right),$$
$$\eta_2 = 1 + \exp\left(2idq_{z,p}^{(2)}\right),$$
$$\eta_3 = -1 + \exp\left(2ihq_{z,p}^{(3)}\right),$$
$$\eta_4 = 1 + \exp\left(2ihq_{z,p}^{(3)}\right),$$
$$\eta_5 = \eta_3 q_{z,p}^{(3)}\sigma_{\mathrm{gr}} - \eta_4\varepsilon_0\varepsilon_3\omega,$$
$$\eta_6 = \eta_3\varepsilon_2\varepsilon_0\omega.$$

In the second step of the approach, we form the integral equations with respect to the current densities in DGG fingers. In the plane of the DGG $z = d$, we write Ohm's law in real space as

$$I_x(x,d) = \sigma(x,d)E_x(x,d),$$
(A6)

where I_x is the current density in the DGG plane and

$$\sigma(x,d) = \begin{cases} \sigma_M & \text{at } 0 < x \leq w_1, \\ 0 & \text{at } w_1 < x \leq w_1 + s_1, \\ \sigma_M & \text{at } w_1 + s_1 < x \leq w_1 + s_1 + w_2, \\ 0 & \text{at } w_1 + s_1 + w_2 < x \leq L, \end{cases}$$
(A7)

with σ_M being the surface conductivity of metal. Using Eqs. (A5)–(A7) and the Fourier inversion, we form two integral equations for the oscillation current densities in DGG fingers as follows:

$$I_x^{(w_1)}(x,d) - \sigma_M 2\frac{\varepsilon_0\varepsilon_1\omega}{q_{z,0}^{(1)}}\exp\left(-iq_{z,0}^{(1)}d\right)Z_0 E_x^{\mathrm{inc}}$$
$$= \int_0^{w_1} I_x^{(w_1)}(x',d)G(x,x')dx'$$
$$+ \int_{w_1+s_1}^{w_1+s_1+w_2} I_x^{(w_2)}(x',d)G(x,x')dx',$$

$$I_x^{(w_2)}(x,d) - \sigma_M 2\frac{\varepsilon_0\varepsilon_1\omega}{q_{z,0}^{(1)}}\exp\left(-iq_{z,0}^{(1)}d\right)Z_0 E_x^{\mathrm{inc}}$$
$$= \int_0^{w_1} I_x^{(w_1)}(x',d)G(x,x')dx'$$
$$+ \int_{w_1+s_1}^{w_1+s_1+w_2} I_x^{(w_2)}(x',d)G(x,x')dx', \quad \text{(A8)}$$

where $I_x^{(w_1)}(x,d)$ and $I_x^{(w_2)}(x,d)$ are the electric current densities in gate fingers w_1 and w_2 and, correspondingly,

$$G(x,x') = \frac{1}{L}\sigma_M \sum_{p=-\infty}^{\infty} Z_p(\sigma_{\mathrm{gr}})\exp\left[iq_p\left(x - x'\right)\right] \quad \text{(A9)}$$

are the kernels of the integrals.

At the third step of the approach, we solve the system of integral equations (A8) by the Galerkin method with expansion of the current densities in the DGG fingers into series of the orthogonal Legendre polynomials

$$I_x^{(w_1)}(x,d) = \sum_{\beta=0}^{\infty} a_\beta^{(1)} P_\beta(\rho_1),$$
$$I_x^{(w_2)}(x,d) = \sum_{\beta=0}^{\infty} a_\beta^{(2)} P_\beta(\rho_2),$$
(A10)

where $a_\beta^{(n)}$ are the expansion coefficients, $P_\beta(\rho_n)$ are the Legendre polynomials, and $\rho_1 = 2x/w_1 - 1$ and $\rho_2 = 2(x - w_1 - s_1)/w_2 - 1$ ($-1 < \rho_n < 1$). Substitution of expansions (A10) into the system of integral equations (A8) transforms it into an infinite system of linear algebraic equations for coefficients $a_\beta^{(n)}$. Based on the convergence of this numerical procedure, we truncate the system of the algebraic equations for $\beta < \beta_0$ and solve it numerically. Finally, upon finding the current densities by solving Eq. (A8), and using Eq. (A5) and the Maxwell equations in each media, we can calculate the induced electric and magnetic fields at an arbitrary point of the structure.

[1] A. N. Grigorenko, M. Polini, and K. S. Novoselov, Graphene plasmonics, Nat. Photonics **6**, 749 (2012).

[2] F. H. L. Koppens, T. Mueller, P. Avouris, A. C. Ferrari, M. S. Vitiello, and M. Polini, Photodetectors based on graphene, other two-dimensional materials and hybrid systems, Nat. Nanotech. **9**, 780 (2014).

[3] F. J. García de Abajo, Graphene plasmonics: Challenges and opportunities, ACS Photonics **1**, 135 (2014).

[4] T. Low and P. Avouris, Graphene plasmonics for terahertz to mid-infrared applications, ACS Nano **8**, 1086 (2014).

[5] Y. Fan, N.-H. Shen, F. Zhang, Q. Zhao, H. Wu, Q. Fu, Z. Wei, H. Li, and C. M. Soukoulis, Graphene plasmonics: A platform for 2D optics, Adv. Optical Mater. **7**, 1800537 (2018).

[6] A. K. Geim and I. V. Grigorieva, Van der Waals heterostructures, Nature **499**, 419 (2013).

[7] A. Woessner, M. B. Lundeberg, Y. Gao, A. Principi, P. Alonso-González, M. Carrega, K. Watanabe, T. Taniguchi, G. Vignale, M. Polini, J. Hone, R. Hillenbrand, and F. H. L. Koppens, Highly confined low-loss plasmons in graphene–boron nitride heterostructures, Nat. Mater. **14**, 421 (2014).

[8] A. S. Mayorov, R. V. Gorbachev, S. V. Morozov, L. Britnell, R. Jalil, L. A. Ponomarenko, P. Blake, K. S. Novoselov, K. Watanabe, T. Taniguchi, and A. K. Geim, Micrometer-scale ballistic transport in encapsulated graphene at room temperature, Nano Lett. **11**, 2396 (2011).

[9] P. J. Zomer, S. P. Dash, N. Tombros, and B. J. van Wees, A transfer technique for high mobility graphene devices on commercially available hexagonal boron nitride, Appl. Phys. Lett. **99**, 232104 (2011).

[10] D. Svintsov, V. Vyurkov, S. Yurchenko, T. Otsuji, and V. Ryzhii, Hydrodynamic model for electron-hole plasma in graphene, J. Appl. Phys. **111**, 083715 (2012).

[11] T. Zhao, S. Gong, M. Hu, R. Zhong, D. Liu, X. Chen, P. Zhang, X. Wang, C. Zhang, P. Wu, and S. Liu, Coherent and tunable terahertz radiation from graphene surface plasmon polarirons excited by cyclotron electron beam, Sci. Rep. **5**, 16059 (2015).

[12] O. V. Polischuk, D. V. Fateev, T. Otsuji, and V. V. Popov, Plasmonic amplification of terahertz radiation in a periodic graphene structure with the carrier injection, Appl. Phys. Lett. **111**, 081110 (2017).

[13] D. V. Fateev, K. V. Mashinsky, and V. V. Popov, Terahertz plasmonic rectification in a spatially periodic graphene, Appl. Phys. Lett. **110**, 061106 (2017).

[14] O. V. Polischuk, V. S. Melnikova, and V. V. Popov, Giant cross-polarization conversion of terahertz radiation by plasmons in an active graphene metasurface, Appl. Phys. Lett. **109**, 131101 (2016).

[15] V. Ryzhii, Terahertz plasma waves in gated graphene heterostructures, Japan, J. Appl. Phys. **45**, L923 (2006).

[16] B. Wunsch, T. Stauber, F. Sols, and F. Guinea, Dynamical polarization of graphene at finite doping, New J. Phys. **8**, 318 (2006).

[17] L. Ju, B. Geng, J. Horng, C. Girit, M. Martin, Z. Hao, H. A. Bechtel, X. Liang, A. Zettl, Y. R. Shen, and F. Wang, Graphene plasmonics for tunable terahertz metamaterials, Nature Nanotech. **6**, 630 (2011).

[18] W. Gao, J. Shu, C. Qiu, and Q. Xu, Excitation of plasmonicwaves in graphene by guided-mode resonances, ACS Nano **6**, 7806 (2012).

[19] W. Gao, G. Shi, Z. Jin, J. Shu, Q. Zhang, R. Vajtai, P. M. Ajayan, J. Kono, and Q. Xu, Excitation and active control of propagating surface plasmon polaritons in graphene, Nano Lett. **13**, 3698 (2013).

[20] H. Yan, X. Li, B. Chandra, G. Tulevski, Y. Wu, M. Freitag, W. Zhu, P. Avouris, and F. Xia, Tunable infrared plasmonic devices using graphene/insulator stacks, Nature Nanotech. **7**, 330 (2012).

[21] Y. Fan, N.-H. Shen, F. Zhang, Q. Zhao, Z. Wei, P. Zhang, J. Dong, Q. Fu, H. Li, and C. M. Soukoulis, Photoexcited graphene metasurfaces: Significantly enhanced and tunable magnetic resonances, ACS Photonics **5**, 1612 (2018).

[22] Z. Wei, H. Li, C. Wu, Y. Cao, J. Ren, Z. Hang, H. Chen, D. Zhang, and C. T. Chan, Anomalous reflection from hybrid metamaterial slab, Opt. Express **18**, 12119 (2010).

[23] R. Alaee, M. Farhat, C. Rockstuhl, and F. Lederer, A perfect absorber made of a graphene micro-ribbon metamaterial, Opt. Express **20**, 28017 (2012).

[24] Z. Fei, A. S. Rodin, G. O. Andreev, W. Bao, A. S. McLeod, M.Wagner, L. M. Zhang, Z. Zhao, M. Thiemens, G. Dominguez, M. M. Fogler, A. H. C. Neto, C. N. Lau, F. Keilmann, and D. N. Basov, Gate-tuning of graphene plasmons revealed by infrared nano-imaging, Nature **487**, 82 (2012).

[25] P. Alonso-González, A. Y. Nikitin, Y. Gao, A. Woessner, M. B. Lundeberg, A. Principi, N. Forcellini, W. Yan, S. Vélez, A. J. Huber, K. Watanabe, T. Taniguchi, F. Casanova, L. E. Hueso, M. Polini, J. Hone, F. H. L. Koppens, and R. Hillenbrand, Acoustic terahertz graphene plasmons revealed by photocurrent nanoscopy, Nat. Nanotech. **12**, 31 (2017).

[26] J. Chen, M. Badioli, P. Alonso-Gonzalez, S. Thongrattanasiri, F. Huth, J. Osmond, M. Spasenovic, A. Centeno, A. Pesquera, P. Godignon, A. Z. Elorza, N. Camara, F. J. G. de Abajo, R. Hillenbrand, and F. H. L. Koppens, Optical nano-imaging of gate-tunable graphene plasmons, Nature **487**, 77 (2012).

[27] J. A. Gerber, S. Berweger, B. T. O'Callahan, and M. B. Raschke, Phase-Resolved Surface Plasmon Interferometry of Graphene, Phys. Rev. Lett. **113**, 055502 (2014).

[28] G. X. Ni, A. S. McLeod, Z. Sun, L. Wang, L. Xiong, K. W. Post, S. S. Sunku, B.-Y. Jiang, J. Hone, C. R. Dean, M. M. Fogler, and Basov, Fundamental limits to graphene plasmonics, Nature **557**, 530 (2018).

[29] N. Kumada, S. Tanabe, H. Hibino, H. Kamata, M. Hashisaka, K. Muraki, and T. Fujisawa, Plasmon transport in graphene investigated by time-resolved electrical measurements, Nat. Commun. **4**, 1363 (2013).

[30] L. Du and D. Tang, Manipulating propagating graphene plasmons at near field by shaped graphene nano-vacancies, J. Opt. Soc. Am. A **31**, 691 (2014).

[31] T. Wenger, G. Viola, J. Kinaret, M. Fogelstrom, and P. Tassin, Current-controlled light scattering and asymmetric plasmon propagation in graphene, Phys. Rev. B **97**, 085419 (2018).

[32] F. Liu, C. Qian, and Y. D. Chong, Directional excitation of graphene surface plasmons, Opt. Express **23**, 2383 (2015).

[33] Y. V. Bludov, M. I. Vasilevskiy, and N. M. R. Peres, Tunable graphene-based polarizer, J. Appl. Phys. **112,** 084320 (2012).

[34] Y. V. Bludov, A. Ferreira, N. M. R. Peres, and M. I. Vasylevskiy, A primer on surface plasmon-polaritons in graphene, Int. J. Mod. Phys. B **27,** 1341001 (2013).

[35] A. Y. Nikitin, P. Alonso-González, and R. Hillenbrand, Efficient coupling of light to graphene plasmons by compressing surface polaritons with tapered bulk materials, Nano Lett. **14,** 2896 (2014).

[36] S. Vantasin, Y. Y. Tanaka, and T. Shimura, Launching and control of graphene plasmon by nanoridge structures, ACS Photonics **5,** 1050 (2017).

[37] T. J. Constant, S. M. Hornett, D. E. Chang, and E. Hendry, All-optical generation of surface plasmons in graphene, Nat. Phys. **12,** 124 (2016).

[38] V. V. Popov, D. V. Fateev, E. L. Ivchenko, and S. D. Ganichev, Noncentrosymmetric plasmon modes and giant terahertz photocurrent in a two-dimensional plasmonic crystal, Phys. Rev. B **91,** 235436 (2015).

[39] G. R. Aizin, V. V. Popov, and O. V. Polischuk, Plasmon enhanced electron drag and terahertz photoconductance in a grating-gated field-effect transistor with two-dimensional electron channel, Appl. Phys. Lett. **89,** 143512 (2006).

[40] P. Olbrich, J. Kamann, M. Konig, J. Munzert, L. Tutsch, J. Eroms, D. Weiss, M.-H. Liu, L. E. Golub, E. L. Ivchenko, V. V. Popov, D. V. Fateev, K. V. Mashinsky, F. Fromm, T. Seyller, and S. D. Ganichev, Terahertz ratchet effects in graphene with a lateral superlattice, Phys. Rev. B **93,** 075422 (2016).

[41] O. V. Polischuk, D. V. Fateev, and V. V. Popov, Amplification of terahertz radiation in a plasmon n-i-p-i graphene structure with charge-carrier injection, Semiconductors **51,** 1460 (2017).

[42] L. A. Falkovsky and A. A. Varlamov, Space-time dispersion of graphene conductivity, Eur. Phys. J. B **56,** 281 (2007).

[43] M. S. Jang, V. W. Brar, M. C. Sherrott, J. J. Lopez, L. Kim, S. Kim, M. Choi, and H. A. Atwater, Tunable large resonant absorption in a midinfrared graphene salisbury screen, Phys. Rev. B **90,** 165409 (2014).

[44] M. Jablan, H. Buljan, and M. Soljačić, Plasmonics in graphene at infrared frequencies, Phys. Rev. B **80,** 245435 (2009).

[45] V. V. Popov, O. V. Polischuk, T. V. Teperik, X. G. Peralta, S. J. Allen, N. J. M. Horing, and M. C. Wanke, Absorption of terahertz radiation by plasmon modes in a grid-gated double-quantum-well field-effect transistor, J. Appl. Phys. **94,** P3556 (2003).